Q Queen's University
Belfast

Benchmarking a modified version of the civ3 nonrelativistic atomic-structure code within Na-like-tungsten R -matrix calculations

Published in:
Physical Review A (Atomic, Molecular, and Optical Physics)

Document Version:
Peer reviewed version

Queen's University Belfast - Research Portal:
Link to publication record in Queen's University Belfast Research Portal

Benchmarking a modified version of CIV3 within Na-like Tungsten R-matrix calculations

M. D. Turkington, C. P. Ballance, A. Hibbert & C. A. Ramsbottom

School of Mathematics and Physics, Queen's University Belfast, Belfast BT7 1NN, Northern Ireland, UK*

In this work we explore the validity of employing a modified version of the non-relativistic structure code CIV3 for heavy, highly charged systems, using Na-like tungsten as a simple benchmark. Consequently, we present radiative and subsequent collisional atomic data compared with corresponding results from a fully-relativistic structure and collisional model. Our motivation for this line of study is to benchmark CIV3 against the relativistic GRASP^0 structure code. This is an important study as CIV3 wavefunctions in non-relativistic R-matrix calculations are computationally less expensive than their Dirac counterparts.

There are very few existing data for the w LXIV ion in the literature with which we can compare except for an incomplete set of energy levels available from the NIST database. The overall accuracy of the present results is thus determined by the comparison between the CIV3 and GRASP^0 structure codes alongside collisional atomic data computed by the R-matrix Breit-Pauli and Dirac codes. It was found that the electron-impact collision strengths and effective collision strengths computed by these differing methods were in good general agreement for the majority of the transitions considered, across a broad range of electron temperatures.

I. INTRODUCTION

The ITER tokamak is a defining landmark on the road to the world's first commercial fusion reactor. The choice of material to be used in the plasma facing components of the divertor region of the reactor was a difficult one, as there are only a few elements that can withstand temperatures of 20-30 keV, consistent with the operating parameters of ITER. It is now certain that the reactor will use tungsten as the plasma facing material [1], owing to its high melting point and thermal conductivity and low sputtering rate. Regardless, tungsten from the plasma facing components of the tokamak will enter the plasma in various ion stages, and this impurity must be characterised. The presence of such impurities has the effect of increasing power losses by producing line emission in the x-ray and EUV regions. Thus, atomic data concerning all stages of tungsten ionization are necessary for diagnostic applications. To this end, the paucity of radiative and collisional data has been urgently addressed in the last decade in works by Ballance *et al.*[2], Safronova *et al.*[3] and Aggarwal *et al.*[4].

In this work we have calculated energy levels, transition rates, collision strengths and Maxwellian averaged effective collision strengths for the W LXIV ion. Due to the presence of only one valence electron, we were able to consider all hydrogenic-like levels up to the $2p^65g\ ^2G$ configuration, while including only 21 fine structure levels. Hence it was not computationally expensive to calculate and retain radiative and collisional data for all transitions between these levels.

To date there have been very few publications concerning the W LXIV ion. The largest theoretical calculation we are aware of was carried out by Kramida and Shirai [5]

and computed theoretical energy levels up to the $2p^65g$ ^2G configuration. In addition, Dipti *et al.*[6] presented energy levels and radiative data for transitions from the $2p^63s\ ^2S_{1/2}$ ground state to several $2p^53l3l'$ configurations, using observations from an EBIT source and from calculations adopting relativistic distorted wave (RDW) theory.

The calculations presented here were carried out using two different methods. Initially the configuration interaction CIV3 code [7, 8] was utilised, incorporating the Breit-Pauli approximation to the relativistic Hamiltonian. In a second evaluation the fully relativistic GRASP^0 code [9–11] was adopted. The reason for using these two separate structure codes was two-fold. First and foremost, we wished to see if the wavefunctions derived from the non-relativistic orbital parameters computed in the CIV3 code, which was designed for calculations involving lowly ionized intermediate-Z ions, could produce accurate structural atomic data for the heavy, highly-ionized W LXIV ion. In both evaluations, we included the $2p^6nl$ n=3,4,5 l=s,p,d,f,g configurations, which led to a total of 210 individual forbidden and allowed transitions. A benefit of being able to obtain precise atomic data from CIV3 is that the orbital parameters can be incorporated in the R-matrix transformation methods ICFT [12] and RMATRX II [13]. These codes require substantially less computational facilities than the fully relativistic DARC suite, a desirable feature because all ionisation stages of the tungsten are required for ITER plasma diagnostics, constituting a considerable effort. Secondly, due to the sparsity of experimental or theoretical data for this ion, we decided that having two sets of data with which to compare would help to discern the validity of our calculations.

The remainder of the paper is as follows. In Section II, we present a summary of the relevant configuration interaction theory employed. Tabulations of energy levels and transition rates are presented, and comparisons

---

* mturkington03@qub.ac.uk

are made between the results from the CIV3 and GRASP[0] codes. Section III outlines the basic collisional Breit-Pauli and Dirac R-matrix theories. We present the collision strengths and Maxwellian averaged effective collision strengths for a selection of allowed and forbidden transitions over a wide range of electron temperatures of importance. In Section IV we derive photon emissivity coefficients (PECs) for the twenty strongest transitions in our model. Finally in Section V we draw conclusions about the viability of the employed methods, the accuracy of the atomic data produced and discuss the goals of future research.

II. THE STRUCTURE CALCULATIONS

A. CIV3 calculations

In the configuration interaction method the total wavefunction describing the target ion is expressed as the sum of a set of configuration state functions (CSFs) $\Phi_i(\alpha_i\pi)$

$$\Psi(J\pi) = \sum_{i}^{M} a_i \Phi_i(\alpha_i J\pi) \qquad (1)$$

where the $\{a_i\}$ are the CI expansion coefficients and α_i denotes the angular momentum coupling scheme used. For a specific set of CSFs, the expansion coefficients are the components of the eigenvectors of the Hamiltonian matrix with elements $< \Phi_i|H|\Phi_j >$. The CSFs are constructed from one-electron orbitals, composed of radial, angular and spin components. In CIV3 each radial function is represented as a linear combination of normalized Slater-type orbitals

$$P_{nl}(r) = \sum_{j=1}^{k} c_{jnl} \left[\frac{(2\zeta_{jnl})^{2I_{jnl}+1}}{(2I_{jnl})!} \right] r^{I_{jnl}} \exp(-\zeta_{jnl}r). \quad (2)$$

An orthonormality condition is imposed on the radial functions such that

$$\int_{0}^{\infty} P_{nl}(r)P_{n'l}(r)\mathrm{d}r = \delta_{nn'}. \qquad (3)$$

If the energy eigenvalues E_i of the Hamiltonian matrix are ordered such that $E_i < E_{i+1}$, then

$$E_i > E_i^{exact} \qquad (4)$$

where the 'exact' energy eigenvalue corresponds to that of the coupling scheme adopted [14]. These form variational principles from which the radial functions may be optimised. During a typical optimisation, we keep the powers of the radial distance I_{jnl} fixed and allow the exponents ζ_{jnl} and the coefficients c_{jnl} to vary freely, subject to (3). For a highly ionised heavy system such as the W LXIV ion, relativistic effects play a crucial role. CIV3 accounts for such effects by supplementing

TABLE I. Optimisation of the orbital parameters.

Orbital	Optimised on energy of	
1s	HF from $5d^46s$ ^{6}D ground state of W II	
2s,3d	$2p^63d$ ^{2}D	
2p,3s	$2p^63s$ ^{2}S	
4s	$2p^64s$ ^{2}S	
5s	$2p^65s$ ^{2}S	
3p	$2p^63p$ ^{2}P^o	
4p	$2p^64p$ ^{2}P^o	(+mass-correction)
5p	$2p^65p$ ^{2}P^o	(+mass-correction)
4d	$2p^64d$ ^{2}D	(+mass-correction)
5d	$2p^65d$ ^{2}D	(+mass-correction)
4f	$2p^64f$ ^{2}F^o	
5f	$2p^65f$ ^{2}F^o	(+mass-correction)
5g	$2p^65g$ ^{2}G	(+mass-correction)

the non-relativistic Schrödinger Hamiltonian with relativistic Breit-Pauli terms; the spin-independent Darwin and mass-correction terms, and the spin-dependent spin-orbit, spin-other-orbit and spin-spin interactions.

B. Radial function parameters

We outline in Table I the optimisation procedures adopted in the present CIV3 evaluation for the 15 spectroscopic orbitals included in the representation of the wavefunction expansions of the target ion. The radial parameters for the 1s core orbital were chosen to be the Hartree-Fock values for the $5d^46s$ ^{6}D ground state of the W II given by McLean and McLean [15]. The parameters for the remaining orbitals were obtained in the following manner. For 2s and 2p we initially chose the Hartree-Fock values of the ground state of the W II given in [15], but these were then reoptimised. The optimal 1s orbital is largely unchanged as the number of electrons in the outer shell varies, so we did not reoptimise the 1s radial function for this 11-electron ion from that of the 73-electron ion. The parameters for 2s, along with 3d, were optimised on the energy of the $2p^63d$ ^{2}D state, while for 2p, along with 3s, we optimised on the energy of the $2p^63s$ ^{2}S state. The remaining orbitals nl were optimised on the energy of the $2p^6nl$ state, in some cases (for $l > 0$) with the mass-correction operator included so as to capture the relativistic contraction of these outer orbitals. Additionally, we made further small adjustments to some of the radial function exponents in order to improve the fine structure splitting between the states. The radial parameters (c_{jnl}, I_{jnl}, ζ_{jnl}) for all the orbitals are tabulated in Table II.

C. Determination of orbitals using GRASP[0]

GRASP[0] is a relativistic atomic structure package used

TABLE II. Radial parameters for the W LXIV used in the CIV3 calculation.

nl	$\langle r \rangle$	c_{jnl}	I_{jnl}	ζ_{jnl}	nl	$\langle r \rangle$	c_{jnl}	I_{jnl}	ζ_{jnl}
1s	0.02047	0.91256	1	75.23257	3p	0.17486	-0.07384	2	44.51621
		0.10554	1	49.16634			0.76941	2	34.70192
		-0.07759	2	36.59489			0.00306	3	142.91730
		0.06448	2	32.00313			-0.74804	3	21.06759
		-0.01735	3	21.91011			0.26460	4	20.16670
		0.01199	3	18.74558			-0.73361	4	24.81636
		-0.00169	4	11.97154	4p	0.33816	0.44859	2	30.54922
		0.00088	4	8.92014			-0.92782	2	33.60156
2s	0.08496	0.01972	1	65.76270			-0.99885	3	21.06719
		0.57967	1	49.70330			2.23243	3	20.83745
		-0.44945	2	36.63235			77.24795	4	11.11203
		-0.85345	2	32.19828			-78.50060	4	11.19057
		0.00689	3	24.38799	5p	0.55857	0.76517	2	15.94698
		0.00453	3	23.07372			0.70228	2	15.77001
		0.00000	4	774.34820			2.34980	3	17.39925
		0.00536	4	90.56360			-7.83165	3	16.09765
3s	0.23817	-0.00346	1	81.22177			9.07239	4	15.24309
		-0.25787	1	49.16634			-5.48755	4	12.15569
		-0.42615	2	36.59261	3d	0.16253	-0.55012	3	23.50000
		1.25424	2	32.00392			-0.48080	3	18.84293
		0.10163	3	26.53384			0.03728	4	13.28512
		-1.66085	3	17.82918			-0.01092	4	7.42249
		2.55623	4	15.58640			0.00484	5	5.56410
		-2.32442	4	14.55794			-0.00127	5	3.69628
4s	0.31345	0.00169	1	83.58593	4d	0.33119	-2.59053	3	19.44456
		0.30979	1	48.73363			4.46604	3	19.08265
		0.56732	2	37.32465			-2.79971	4	16.67027
		-1.63220	2	31.85813			-0.15987	4	33.65818
		-1.94461	3	22.87161			-4.98899	5	17.39352
		2.59965	3	22.65146			5.59115	5	17.76746
		1.25897	4	25.31327	5d	0.52481	0.20406	3	27.43470
		-1.45809	4	14.37310			0.49988	3	17.88940
5s	0.54460	-0.00900	1	76.93152			-0.01110	4	30.18838
		0.16758	1	48.87097			0.01488	4	29.88650
		0.25279	2	38.89847			-2.47602	5	16.78989
		-0.90173	2	30.92275			2.34067	5	12.25650
		175.24223	3	11.21427	4f	0.27111	-0.99252	4	16.73106
		-227.08973	3	10.26120			-0.02383	4	5.83540
		-631.10285	4	11.54065	5f	0.50092	1.94693	4	14.90661
		687.49737	4	11.42525			-2.30768	4	11.02760
2p	0.07144	0.08821	2	49.81390	5g	0.42952	1.02078	5	12.78938
		0.90932	2	33.95499			-0.02088	5	12.05930
		0.01277	3	39.84916					
		-0.00652	3	21.97709					
		0.00357	4	21.23783					
		-0.00027	4	11.84366					

to generate relativistic orbitals within the MCDF (Multi-Configuration Dirac-Fock) approximation. In particular the 25 relativistic orbitals emplyed in our model were obtained from a Dirac-Coulomb Hamiltonian of the form

$$H_D = \sum_i \left(c\boldsymbol{\alpha}.\boldsymbol{p}_i + (\boldsymbol{\beta} - 1)c^2 - \frac{Z}{r_i} \right) + \sum_{i>j=1} \frac{1}{r_{ij}}. \quad (5)$$

Here the electrons are labelled i and j, $\boldsymbol{\alpha}$ and $\boldsymbol{\beta}$ are matrices associated with the Pauli spin matrices, $\boldsymbol{p}_i$ is

the electron momentum operator, c is the speed of light and Z is the atomic number. Unlike the orbitals derived using CIV3, these relativistic orbitals are formed from a large component, $\mathcal{P}_{nl}$ and small component $\mathcal{Q}_{nl}$. The orbitals were not optimised on any subset of levels, but on the average of the best minimisation of all levels. The GRASP[0] values are used as the benchmark by which CIV3 is compared.

D.   Radiative Atomic Data

We list in Table III the energy levels in Rydbergs for the lowest 21 fine-structure terms, relative to the $2p^6 3s$ ^2S ground state of W LXIV, evaluated in the present 12-configuration model. Comparisons are made between energies derived from the orbitals in CIV3 as discussed in the previous subsection, those from the orbitals determined using the fully relativistic GRASP^0 package and the separations available in the NIST database [5]. Considering the fully relativistic GRASP^0 energies first, we see that there is quite good agreement with NIST for all fine structure levels. Since this is a structure code specifically designed to deal with cases where relativistic effects are important, this agreement is to be expected. More surprising is the extent of the agreement between CIV3, GRASP^0 and NIST, since CIV3 is not a fully relativistic code. The best alignment occurs for the $n=3$ levels with somewhat higher disparities evident for the $n=4$ and $n=5$ states. This is due to the difference between the fully relativistic and CIV3 orbitals.

TABLE III. Energy levels (in Ryds) relative to the $2p^6 3s$ ^2S ground state of W LXIV from CIV3, GRASP0 and NIST [5].

Index	Config	Term	J	CIV3	NIST	GRASP^0
1	$2p^6 3s$	^2S	0.5	0.00	0.00	0.00
2	$2p^6 3p$	$^2P^o$	0.5	11.59	11.73	11.87
3			1.5	38.49	39.19	39.63
4	$2p^6 3d$	^2D	1.5	53.69	52.97	53.53
5			2.5	59.68	59.21	59.93
6	$2p^6 4s$	^2S	0.5	240.70	239.12	239.56
7	$2p^6 4p$	$^2P^o$	0.5	247.83	243.92	244.46
8			1.5	258.82	255.18	255.82
9	$2p^6 4d$	^2D	1.5	261.66	260.37	261.11
10			2.5	264.37	263.09	263.87
11	$2p^6 4f$	$^2F^o$	2.5	267.57	265.94	266.50
12			3.5	268.85	267.09	267.84
13	$2p^6 5s$	^2S	0.5	349.09	-	346.74
14	$2p^6 5p$	$^2P^o$	0.5	349.29	-	348.53
15			1.5	354.65	-	354.23
16	$2p^6 5d$	^2D	1.5	357.81	-	356.83
17			2.5	359.00	357.54	358.25
18	$2p^6 5f$	$^2F^o$	2.5	360.54	358.84	359.63
19			3.5	361.14	359.46	360.24
20	$2p^6 5g$	^2G	3.5	361.65	359.77	360.43
21			4.5	361.70	360.11	360.80

We present in Table IV the transition rates (A-values) for several fine-structure E1 transitions in the W LXIV ion, calculated using theoretical energies. In this case, we are only able to compare the results of our CIV3 and GRASP^0 calculations, since to the best of our knowledge, there are no other data with which to compare. Comparison of the two sets of calculations shows that for the majority of the E1 transitions there is generally quite good agreement; in some cases the agreement is very good. The greatest disparities occur for the $3p$ $^2P^o_{1/2}$ - $5s$ $^2S_{1/2}$,

$3p$ $^2P^o_{3/2}$ - $5d$ $^2D_{3/2}$ and $3d$ $^2D_{3/2}$ - $5p$ $^2P^o_{1/2}$ transitions. These large differences have been traced back to spurious CI cancellations in the CIV3 calculation, arising because the CIV3 radial functions are not fully relativistic.

TABLE IV. Comparison of A-values (in s^{-1}) for E1 fine-structure transitions between CIV3 and GRASP0. Numbers in square brackets represent powers of 10.

Upper Level	Lower level	A-value CIV3	GRASP^0
$3s$ $^2S_{1/2}$	$3p$ $^2P^o_{1/2}$	4.19[10]	4.52[10]
$3s$ $^2S_{1/2}$	$3p$ $^2P^o_{3/2}$	1.62[12]	1.82[12]
$3s$ $^2S_{1/2}$	$4p$ $^2P^o_{1/2}$	5.06[13]	6.20[13]
$3s$ $^2S_{1/2}$	$4p$ $^2P^o_{3/2}$	3.30[13]	3.80[13]
$3s$ $^2S_{1/2}$	$5p$ $^2P^o_{1/2}$	2.33[13]	3.33[13]
$3s$ $^2S_{1/2}$	$5p$ $^2P^o_{3/2}$	2.02[13]	2.29[13]
$3p$ $^2P^o_{1/2}$	$3d$ $^2D_{3/2}$	1.47[12]	1.49[12]
$3p$ $^2P^o_{1/2}$	$4s$ $^2S_{1/2}$	1.12[13]	1.66[13]
$3p$ $^2P^o_{1/2}$	$4d$ $^2D_{3/2}$	8.21[13]	9.14[13]
$3p$ $^2P^o_{1/2}$	$5s$ $^2S_{1/2}$	2.92[11]	7.82[12]
$3p$ $^2P^o_{1/2}$	$5d$ $^2D_{3/2}$	3.10[13]	5.11[13]
$3p$ $^2P^o_{3/2}$	$3d$ $^2D_{3/2}$	1.43[10]	1.09[10]
$3p$ $^2P^o_{3/2}$	$3d$ $^2D_{5/2}$	2.45[11]	2.12[11]
$3p$ $^2P^o_{3/2}$	$4s$ $^2S_{1/2}$	4.35[13]	4.86[13]
$3p$ $^2P^o_{3/2}$	$4d$ $^2D_{3/2}$	1.91[13]	2.07[13]
$3p$ $^2P^o_{3/2}$	$4d$ $^2D_{5/2}$	1.11[14]	1.18[14]
$3p$ $^2P^o_{3/2}$	$5s$ $^2S_{1/2}$	1.95[13]	2.20[13]
$3p$ $^2P^o_{3/2}$	$5d$ $^2D_{3/2}$	9.92[12]	1.03[13]
$3p$ $^2P^o_{3/2}$	$5d$ $^2D_{5/2}$	6.20[13]	6.09[13]
$3d$ $^2D_{3/2}$	$4p$ $^2P^o_{1/2}$	1.43[13]	1.64[13]
$3d$ $^2D_{3/2}$	$4p$ $^2P^o_{3/2}$	7.14[11]	9.18[11]
$3d$ $^2D_{3/2}$	$4f$ $^2F^o_{5/2}$	2.36[14]	2.31[14]
$3d$ $^2D_{3/2}$	$5p$ $^2P^o_{1/2}$	2.59[12]	6.70[12]
$3d$ $^2D_{3/2}$	$5p$ $^2P^o_{3/2}$	8.59[10]	3.85[11]
$3d$ $^2D_{3/2}$	$5f$ $^2F^o_{5/2}$	7.28[13]	8.09[13]
$3d$ $^2D_{5/2}$	$4p$ $^2P^o_{3/2}$	8.70[12]	9.57[12]
$3d$ $^2D_{5/2}$	$4f$ $^2F^o_{5/2}$	1.63[13]	1.58[13]
$3d$ $^2D_{5/2}$	$4f$ $^2F^o_{7/2}$	2.47[14]	2.40[14]
$3d$ $^2D_{5/2}$	$5p$ $^2P^o_{3/2}$	2.14[12]	4.00[12]
$3d$ $^2D_{5/2}$	$5f$ $^2F^o_{5/2}$	4.93[12]	5.35[12]
$3d$ $^2D_{5/2}$	$5f$ $^2F^o_{7/2}$	7.82[13]	8.27[13]

Table V shows the A-values for E2 transitions, again using theoretical transition energies, from both the CIV3 and GRASP^0 calculations. One of the most noticeable things about these transitions is that the poorest agreements arise from the $n = 3$ to $n = 5$ cases, again due to the differences in the way the radial functions were obtained.

However, in order to get a more accurate indication of the differences between the CIV3 and GRASP^0 models, their respective energies were shifted to the common NIST values during the course of the collisional calculation. The dipole transition rates are calculated as

$$A = \frac{64\pi^4 e^2 a_0^2 \sigma^3}{3h} \left| \left\langle \gamma J M \left| P_q^{(1)} \right| \gamma' J' M' \right\rangle \right|^2 \quad (6)$$

where a_0 is the Bohr radius, σ is the transition energy, $P_q^{(1)}$ is the qth component of the classical dipole moment of the atom measured in units of ea_0 and $\gamma'J'M'$ and γJM are respectively the energetically higher and lower states involved. When the energy levels of either of our models are shifted to the NIST values, then the E1 transition rates are scaled by a factor of

$$\left(\frac{\Delta E_{NIST}}{\Delta E_{model}}\right)^3. \tag{7}$$

where ΔE denotes the transition energy. The effect of this scaling on the transition rates is given in Table VI. Clearly there are some changes to the transition rates, but these changes are generally small. It is seen therefore that the main difference between the results from the CIV3 and GRASP^0 calculations arise from the differ-

ent manner in which relativistic effects are introduced in these two models. Nevertheless, the extent of the agreement is surprisingly good for such a highly ionised ion.

Finally, Table VII shows the scaled E2 A-values. The scaling method is the same as for the electric dipole case, except that the ratio between the energy differences seen in equation (7) is taken to the power of five instead of three.

TABLE V. Comparison of A-values (in s^{-1}) E2 fine-structure transitions between CIV3 and GRASP0. Numbers in square brackets represent powers of 10.

Upper Level	Lower level	A-value	
		CIV3	GRASP^0
3s $^2S_{1/2}$	3d $^2D_{3/2}$	1.45[08]	1.47[08]
3s $^2S_{1/2}$	3d $^2D_{5/2}$	2.60[08]	2.71[08]
3s $^2S_{1/2}$	4d $^2D_{3/2}$	3.92[11]	4.36[11]
3s $^2S_{1/2}$	4d $^2D_{5/2}$	3.96[11]	4.33[11]
3s $^2S_{1/2}$	5d $^2D_{3/2}$	5.26[10]	1.92[11]
3s $^2S_{1/2}$	5d $^2D_{5/2}$	6.02[10]	2.01[11]
3p $^2P^o_{1/2}$	3p $^2P^o_{3/2}$	6.16[06]	7.52[06]
3p $^2P^o_{1/2}$	4p $^2P^o_{3/2}$	7.60[10]	1.10[11]
3p $^2P^o_{1/2}$	4f $^2F^o_{5/2}$	6.23[11]	6.39[11]
3p $^2P^o_{1/2}$	5p $^2P^o_{3/2}$	5.10[08]	6.63[10]
3p $^2P^o_{1/2}$	5f $^2F^o_{5/2}$	7.50[09]	7.12[10]
3p $^2P^o_{3/2}$	4p $^2P^o_{1/2}$	2.15[11]	2.10[11]
3p $^2P^o_{3/2}$	4p $^2P^o_{3/2}$	1.07[11]	1.04[11]
3p $^2P^o_{3/2}$	4f $^2F^o_{5/2}$	1.29[11]	1.30[11]
3p $^2P^o_{3/2}$	4f $^2F^o_{7/2}$	5.96[11]	5.98[11]
3p $^2P^o_{3/2}$	5p $^2P^o_{1/2}$	1.36[11]	9.91[10]
3p $^2P^o_{3/2}$	5p $^2P^o_{3/2}$	8.72[10]	5.66[10]
3p $^2P^o_{3/2}$	5f $^2F^o_{5/2}$	1.15[10]	5.76[09]
3p $^2P^o_{3/2}$	5f $^2F^o_{7/2}$	5.88[10]	3.11[10]
3d $^2D_{3/2}$	3d $^2D_{5/2}$	7.45[02]	8.71[02]
3d $^2D_{3/2}$	4s $^2S_{1/2}$	3.29[10]	3.76[10]
3d $^2D_{3/2}$	4d $^2D_{3/2}$	5.45[10]	6.09[10]
3d $^2D_{3/2}$	4d $^2D_{5/2}$	1.58[10]	1.73[10]
3d $^2D_{3/2}$	5s $^2S_{1/2}$	1.18[09]	2.08[10]
3d $^2D_{3/2}$	5d $^2D_{3/2}$	2.30[09]	2.85[10]
3d $^2D_{3/2}$	5d $^2D_{5/2}$	7.95[08]	8.44[09]
3d $^2D_{3/2}$	5g $^2G_{7/2}$	7.53[11]	7.16[11]
3d $^2D_{5/2}$	4s $^2S_{1/2}$	5.13[10]	5.47[10]
3d $^2D_{5/2}$	4d $^2D_{3/2}$	2.34[10]	2.51[10]
3d $^2D_{5/2}$	4d $^2D_{5/2}$	6.33[10]	6.71[10]
3d $^2D_{5/2}$	5s $^2S_{1/2}$	1.29[09]	2.98[10]
3d $^2D_{5/2}$	5d $^2D_{3/2}$	3.09[09]	1.13[10]
3d $^2D_{5/2}$	5d $^2D_{5/2}$	9.37[09]	3.16[10]
3d $^2D_{5/2}$	5g $^2G_{7/2}$	8.12[10]	7.91[10]
3d $^2D_{5/2}$	5g $^2G_{9/2}$	8.17[11]	7.83[11]

TABLE VI. Comparison of scaled A-values (in s^{-1}) for E1 fine-structure transitions between CIV3 and GRASP0. Numbers in square brackets represent powers of 10.

Upper Level	Lower level	A-value	
		CIV3	GRASP^0
3s $^2S_{1/2}$	3p $^2P^o_{1/2}$	4.33[10]	4.36[10]
3s $^2S_{1/2}$	3p $^2P^o_{3/2}$	1.71[12]	1.76[12]
3s $^2S_{1/2}$	4p $^2P^o_{1/2}$	4.82[13]	6.18[13]
3s $^2S_{1/2}$	4p $^2P^o_{3/2}$	3.16[13]	3.83[13]
3s $^2S_{1/2}$	5p $^2P^o_{1/2}$	2.36[13]	3.40[13]
3s $^2S_{1/2}$	5p $^2P^o_{3/2}$	2.00[13]	2.32[13]
3p $^2P^o_{1/2}$	3d $^2D_{3/2}$	1.39[12]	1.44[12]
3p $^2P^o_{1/2}$	4s $^2S_{1/2}$	1.10[13]	1.67[13]
3p $^2P^o_{1/2}$	4d $^2D_{3/2}$	8.07[13]	9.14[13]
3p $^2P^o_{1/2}$	5s $^2S_{1/2}$	2.82[11]	8.05[12]
3p $^2P^o_{1/2}$	5d $^2D_{3/2}$	3.04[13]	5.12[13]
3p $^2P^o_{3/2}$	3d $^2D_{3/2}$	1.06[10]	1.06[10]
3p $^2P^o_{3/2}$	3d $^2D_{5/2}$	2.01[11]	2.03[11]
3p $^2P^o_{3/2}$	4s $^2S_{1/2}$	4.20[13]	4.86[13]
3p $^2P^o_{3/2}$	4d $^2D_{3/2}$	1.86[13]	2.05[13]
3p $^2P^o_{3/2}$	4d $^2D_{5/2}$	1.08[14]	1.18[14]
3p $^2P^o_{3/2}$	5s $^2S_{1/2}$	1.90[13]	2.24[13]
3p $^2P^o_{3/2}$	5d $^2D_{3/2}$	9.96[12]	1.02[13]
3p $^2P^o_{3/2}$	5d $^2D_{5/2}$	6.06[13]	6.15[13]
3d $^2D_{3/2}$	4p $^2P^o_{1/2}$	1.36[13]	1.65[13]
3d $^2D_{3/2}$	4p $^2P^o_{3/2}$	6.82[11]	9.32[11]
3d $^2D_{3/2}$	4f $^2F^o_{5/2}$	2.33[14]	2.31[14]
3d $^2D_{3/2}$	5p $^2P^o_{1/2}$	2.64[12]	6.94[12]
3d $^2D_{3/2}$	5p $^2P^o_{3/2}$	8.48[10]	3.93[11]
3d $^2D_{3/2}$	5f $^2F^o_{5/2}$	7.21[13]	8.10[13]
3d $^2D_{5/2}$	4p $^2P^o_{3/2}$	8.30[12]	9.60[12]
3d $^2D_{5/2}$	4f $^2F^o_{5/2}$	1.60[13]	1.57[13]
3d $^2D_{5/2}$	4f $^2F^o_{7/2}$	2.43[14]	2.42[14]
3d $^2D_{5/2}$	5p $^2P^o_{3/2}$	2.12[12]	4.00[12]
3d $^2D_{5/2}$	5f $^2F^o_{5/2}$	4.88[12]	5.26[12]
3d $^2D_{5/2}$	5f $^2F^o_{7/2}$	7.73[13]	8.36[13]

III. THE COLLISION CALCULATION

In this section we report on the results from two variants of the R-matrix codes to compute the collision strength Ω_{if} and corresponding effective collision strength Υ_{if} for all transitions among the 21 fine-structure levels of the W LXIV ion. The collision strength between an initial state "i" and a final state "f" is defined

TABLE VII. Comparison of scaled A-values (in s^{-1}) for E2 fine-structure transitions from CIV3 and GRASP0. Numbers in square brackets represent powers of 10.

Upper Level	Lower level	A-value CIV3	A-value GRASP^0
3s ^{2}S$_{1/2}$	3d ^{2}D$_{3/2}$	1.36[08]	1.39[08]
3s ^{2}S$_{1/2}$	3d ^{2}D$_{5/2}$	2.50[08]	2.55[08]
3s ^{2}S$_{1/2}$	4d ^{2}D$_{3/2}$	3.82[11]	4.30[11]
3s ^{2}S$_{1/2}$	4d ^{2}D$_{5/2}$	3.87[11]	4.27[11]
3s ^{2}S$_{1/2}$	5d ^{2}D$_{3/2}$	5.14[10]	1.90[11]
3s ^{2}S$_{1/2}$	5d ^{2}D$_{5/2}$	5.90[10]	1.99[11]
3p ^{2}P$^o_{1/2}$	3p ^{2}P$^o_{3/2}$	6.83[06]	7.12[06]
3p ^{2}P$^o_{1/2}$	4p ^{2}P$^o_{3/2}$	7.04[10]	1.09[11]
3p ^{2}P$^o_{1/2}$	4f ^{2}F$^o_{5/2}$	6.02[11]	6.34[11]
3p ^{2}P$^o_{1/2}$	5p ^{2}P$^o_{3/2}$	5.02[08]	6.59[10]
3p ^{2}P$^o_{1/2}$	5f ^{2}F$^o_{5/2}$	7.30[09]	7.05[10]
3p ^{2}P$^o_{3/2}$	4p ^{2}P$^o_{1/2}$	1.92[11]	2.09[11]
3p ^{2}P$^o_{3/2}$	4p ^{2}P$^o_{3/2}$	9.69[10]	1.04[11]
3p ^{2}P$^o_{3/2}$	4f ^{2}F$^o_{5/2}$	1.23[11]	1.30[11]
3p ^{2}P$^o_{3/2}$	4f ^{2}F$^o_{7/2}$	5.65[11]	5.94[11]
3p ^{2}P$^o_{3/2}$	5p ^{2}P$^o_{1/2}$	1.38[11]	1.04[11]
3p ^{2}P$^o_{3/2}$	5p ^{2}P$^o_{3/2}$	8.50[10]	5.65[10]
3p ^{2}P$^o_{3/2}$	5f ^{2}F$^o_{5/2}$	1.11[10]	5.73[09]
3p ^{2}P$^o_{3/2}$	5f ^{2}F$^o_{7/2}$	5.67[10]	3.09[10]
3d ^{2}D$_{3/2}$	3d ^{2}D$_{5/2}$	9.14[02]	7.67[02]
3d ^{2}D$_{3/2}$	4s ^{2}S$_{1/2}$	3.22[10]	3.77[10]
3d ^{2}D$_{3/2}$	4d ^{2}D$_{3/2}$	5.38[10]	6.06[10]
3d ^{2}D$_{3/2}$	4d ^{2}D$_{5/2}$	1.56[10]	1.72[10]
3d ^{2}D$_{3/2}$	5s ^{2}S$_{1/2}$	1.16[09]	2.13[10]
3d ^{2}D$_{3/2}$	5d ^{2}D$_{3/2}$	2.26[09]	2.84[10]
3d ^{2}D$_{3/2}$	5d ^{2}D$_{5/2}$	7.85[08]	8.42[09]
3d ^{2}D$_{3/2}$	5g ^{2}G$_{7/2}$	7.39[11]	7.15[11]
3d ^{2}D$_{5/2}$	4s ^{2}S$_{1/2}$	4.97[10]	5.51[10]
3d ^{2}D$_{5/2}$	4d ^{2}D$_{3/2}$	2.29[10]	2.51[10]
3d ^{2}D$_{5/2}$	4d ^{2}D$_{5/2}$	6.21[10]	6.70[10]
3d ^{2}D$_{5/2}$	5s ^{2}S$_{1/2}$	1.26[09]	3.06[10]
3d ^{2}D$_{5/2}$	5d ^{2}D$_{3/2}$	3.03[09]	1.13[10]
3d ^{2}D$_{5/2}$	5d ^{2}D$_{5/2}$	9.22[09]	3.16[10]
3d ^{2}D$_{5/2}$	5g ^{2}G$_{7/2}$	7.93[10]	7.92[10]
3d ^{2}D$_{5/2}$	5g ^{2}G$_{9/2}$	8.02[11]	7.83[11]

in terms of the collision cross section σ_{if} by

$$\Omega_{if} = \frac{(2J_i + 1)k_i^2}{\pi}\sigma_{if}. \qquad (8)$$

where $(2J_i + 1)$ is the statistical weight of the initial state and k_i^2 is the scattering channel energy. By averaging these collision strengths over a Maxwellian distribution of electron velocities, we can obtain the corresponding effective collision strength

$$\Upsilon_{if}(T_e) = \int_0^\infty \Omega_{if}(E_f) \exp\left(\frac{-E_f}{kT_e}\right) d\left(\frac{E_f}{kT_e}\right) \qquad (9)$$

where E_f is the final kinetic energy of the scattered electron, T_e is the electron temperature in Kelvin and k is Boltzmann's constant. The calculation of the effective collision strengths employs the integration methods of

Burgess and Tully [16] and above the largest target state threshold the theoretical value of the collision strength was interpolated to the infinite energy limit in the manner discussed by Whiteford *et al.*[17].

Two different sets of codes were employed for the collision calculations. Initially the Breit-Pauli RMATRXI suite [18, 19], which uses the non-relativistic orbitals from the CIV3 model discussed in the previous section, was utilised. This variant of the R-matrix codes employs LS coupling to generate the $(N+1)$-electron matrix elements, and these are then transformed to a jK coupling representation. In contrast, the DARC (Dirac Atomic R-matrix Code) [20] suite uses the fully-relativistic orbitals from the GRASP^0 calculation, and the entirety of the inner region calculations are performed relativistically. The R-matrix boundary was chosen in the former calculation to be 2.3 atomic units (a.u.) and in the latter to be 1.64 a.u. In both calculations the number of continuum orbitals was set to 30 and a very fine mesh (4×10^{-5} scaled Rydbergs) of incident electron energies was employed over the entire region of interest from 0-1600 Ryds. A finer mesh was used in a separate calculation to check if convergence had been achieved in the resonance resolution and it was found that the mesh listed above was perfectly acceptable. A total of 100,000 mesh points were used in both outer region calculations. The outer region code PSTGF [18] allowed for the incorporation of the Burgess-Tully top-up method [21] to account for partial waves ranging from $2J = 80$ to infinity. The effects of radiation damping [22] were also considered but the effects were minimal due to the high temperatures considered in our Maxwellian-averaged collision calculation. Finally, effective collisions strengths were produced for 14 temperatures ranging from 5×10^6 to 9×10^7 K which is the region of peak abundance for this tungsten ion stage.

A. Collisional Atomic Data

In this section collision strengths and effective collision strengths are presented for a variety of allowed and forbidden lines in W LXIV computed using the CIV3 and GRASP^0 models in the RMATRXI and DARC R-matrix suites respectively. The results are compared in order to see the effect and suitability of adopting the different structure models for this highly ionised heavy element. While data for all 210 transitions were calculated, in this paper we present a selection of results for transitions with an initial configuration of $2p^6 3l$, $l = $s,p,d to emphasise our findings.

Figures 1 and 2 show the collision strengths and corresponding Maxwellian averaged effective collision strengths for two strong dipole-transitions, 3s ^{2}S$_{1/2}$ $\rightarrow$ 3p ^{2}P$^o_{1/2}$ (index 1-2) and 3s ^{2}S$_{1/2}$ $\rightarrow$ 4p ^{2}P$^o_{1/2}$ (index 1-7) respectively. Surprisingly close agreement is found for both transitions. The collision strength resonance structures coincide in regard to position and magnitude and the background cross sections show little disparity.
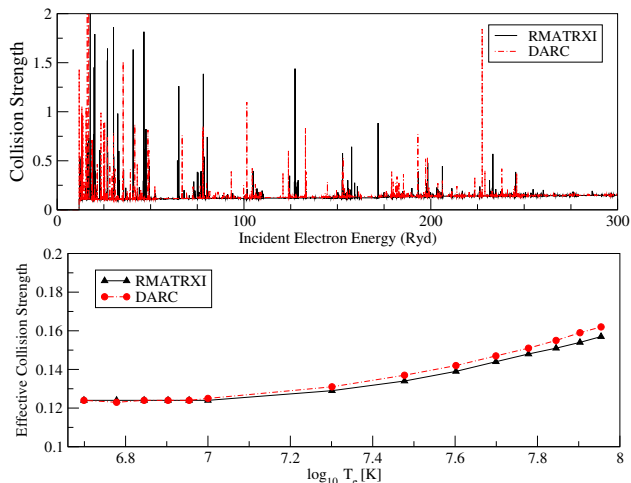
FIG. 1. The collision strengths (upper panel) and the corresponding effective collision strengths (lower panel) for the dipole allowed 3s ^{2}S$_{1/2}$ → 3p ^{2}P$^o_{1/2}$ (index 1-2) transition. Dashed lines, RMATRXI; solid lines, DARC.

In the upper panel in Figure 1 we see on closer analysis that the DARC results consistently lie slightly above those of the RMATRXI calculation. However, these differences, combined with some slight differences in resonance structures in the 120 to 160 Rydberg region, have only a minor effect on the corresponding effective collision strength depicted in the lower panel. The differences amount to an average disparity of 1.37%. This is not an unsurprising result, considering the 0.69% difference in the corresponding scaled transition probability for this transition.

The 3s ^{2}S$_{1/2}$ → 4p ^{2}P$^o_{1/2}$ (index 1-7) transition depicted in Figure 2 is about 30 times weaker than the 1-2 line in Figure 1. On careful inspection of the collision strength
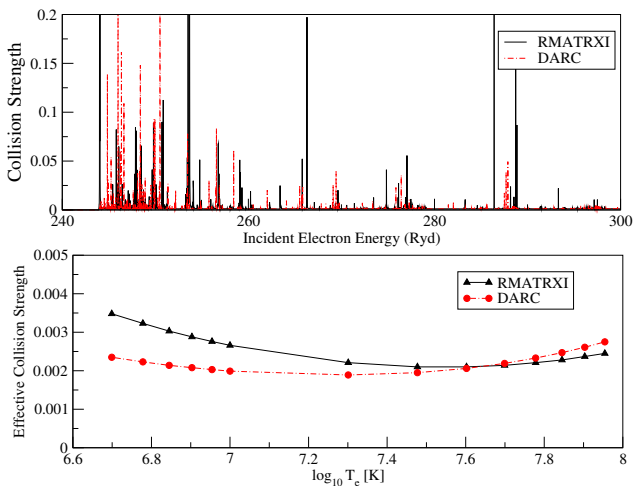

FIG. 2. The collision strengths (upper panel) and the corresponding effective collision strengths (lower panel) for the dipole allowed 3s ^{2}S$_{1/2}$ → 4p ^{2}P$^o_{1/2}$ (index 1-7) transition.

in the upper panel we see that there are several large resonances that appear in the RMATRXI calculation which are absent in the DARC calculation. These additional features augment the corresponding effective collision strength in the low temperature region. Despite these differences the agreement between the two calculations is on average a very acceptable 11%. The cause of these slight disparities appear to stem from the initial structure calculations. Indeed if we look back at the relevant energy levels in Table III, we find that the CIV3 4p level lies approximately 3 Rydbergs above the value proposed by NIST or GRASP^0. It would seem therefore that small differences in structure are significant enough to have an affect, albeit small, on the resulting collision atomic data for this ion.
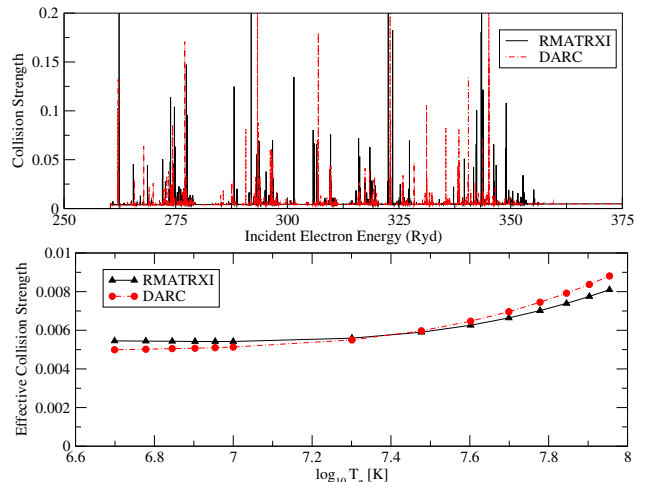

FIG. 3. The collision strengths (upper panel) and the corresponding effective collision strengths (lower panel) for the dipole allowed 3p ^{2}P$^o_{1/2}$ → 4d ^{2}D$_{3/2}$ (index 2-9) transition.

In Figure 3 we present results for another dipole-allowed transition from a metastable initial state 3p ^{2}P$^o_{1/2}$ to the n=4 final state 4d ^{2}D$_{1/2}$ (index 2-9). Similar to the 3s ^{2}S$_{1/2}$ → 4p ^{2}P$^o_{1/2}$ (index 2-7) case this is a relatively weak transition. Excellent agreement, however, is evident between RMATRXI and DARC results for all incident electron energies and for all electron temperatures. On closer inspection it can be seen that the background of the DARC calculation lies very slightly below that of the RMATRXI calculation in the 250 to 300 Rydberg region and a small number of large resonances appear uniquely around the 300 and 350 Rydberg regions in the RMATRXI calculation. These additional features do not, however, significantly affect the corresponding Maxwellian-averaged effective collision strengths seen in the lower panel, for which an average difference of 0.22% was recorded across the entire temperature range.

Thus far we have only considered electric dipole transitions since they represent the strongest lines for the W LXIV ion. The structure evaluations, however, revealed that there were also several strong electric quadrupole transitions with A-values of the order 10^{11}
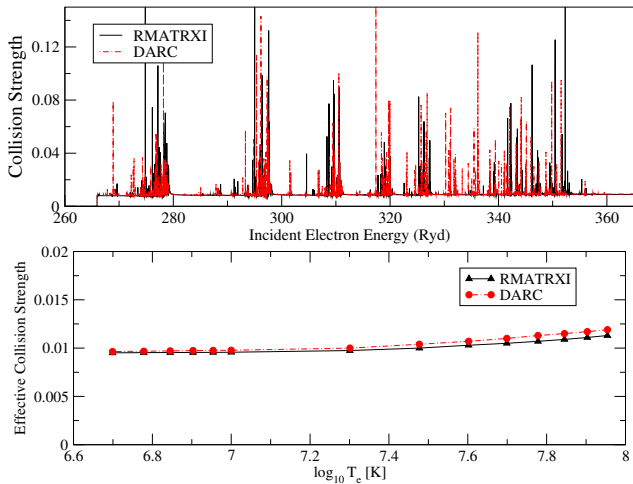
FIG. 4. The collision strengths (upper panel) and the corresponding effective collision strengths (lower panel) for the electric quadrupole 3p ^{2}P$^o_{1/2}$ → 4f ^{2}F$^o_{5/2}$ (index 2-11) transition.
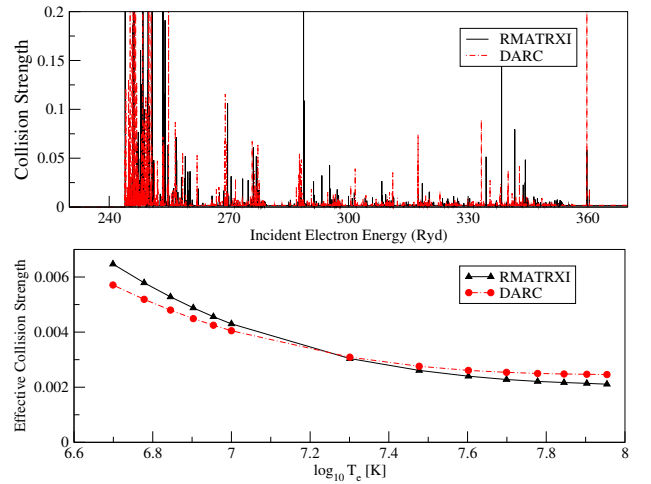

FIG. 5. The collision strengths (upper panel) and the corresponding effective collision strengths (lower panel) for the electric quadrupole 3p ^{2}P$^o_{3/2}$ → 4p ^{2}P$^o_{1/2}$ (index 3-7) transition.

(s^{-1}). We now consider two of these in Figures 4 and 5, the 3p ^{2}P$^o_{1/2}$ → 4f ^{2}F$^o_{5/2}$ (index 2-11) and the 3p ^{2}P$^o_{3/2}$ → 4p ^{2}P$^o_{1/2}$ (index 3-7) electric quadrupole transitions. The scaled transition probabilities were calculated to be 6.02×10^{11} and 6.34×10^{11} for the CIV3 and GRASP^0 models respectively, with a difference of 5.32%. Again extremely good agreement is found between the collision strengths and effective collision strengths across all incident electron energies and electron temperatures. The DARC results consistently lie slightly above those of RMATRXI. The small differences in the resonance structures have little overall effect on the corresponding Maxwellian-averaged effective collisions strengths. The results differ by an average of 3.43%. A complete set of collision strengths and Maxwellian averaged collision strengths for all 210 individual transitions are available from the authors on request.

IV. MODELLING

In the context of the generalized collisional-radiative model (GCR), which properly describes the collisional regime of most astrophysical and laboratory fusion plasmas [23], excitation photon emissivity coefficients ($\mathcal{PEC}$s) associated with ion populations and spectral line emissions for the transition $j \to k$ take the form

$$\mathcal{PEC}^{(\text{exc})}_{\sigma, j \to k} = A_{j \to k} F^{(\text{exc})}_{j\sigma}. \qquad (10)$$

$F^{(\text{exc})}_{j\sigma}$ is the contribution to excited populations due to excitation from the metastable state σ, and $A_{j \to k}$ is the A-value associated with the $j \to k$ transition. Within the Coronal Approximation, which assumes that the only

mechanism by which excited states are populated is collisional excitation and depopulation of these states only occurs by radiative decay, equation (10) can be rewritten as

$$\mathcal{PEC}_{\sigma, j \to k} = \frac{q_{\sigma \to j} A_{j \to k}}{\sum_{i<j} A_{j \to k}} \qquad (11)$$

where $q_{\sigma \to j}$ is the electron-impact excitation rate coefficient from the σth metastable state. Taking the ratio between two of these line intensities is an important tool in plasma diagnostics, as it gives vital information on the temperature or density of the plasma.

Figure 6 shows the results of calculating the photon emissivity coefficients for transitions in the W LXIV ion. It is interesting to note that while four of the five strongest intensities are from strong dipoles, the fifth is from an electric quadrupole transition from the 3d ^{2}D$_{3/2}$ → 4s ^{2}S$_{1/2}$.

V. CONCLUSIONS

In this paper we present energy levels, A-values, collision strengths and effective collision strengths for 210 individual allowed and forbidden lines in the W LXIV ion. The radiative data were evaluated using the CIV3 and GRASP^0 structure codes while the collisional data were computed using the RMATRXI Breit-Pauli and DARC variants of the R-matrix method. Good agreement was found when comparisons of all the atomic data were made. For the majority of the transitions considered, differences of less than 10% were recorded and for many transitions, particularly among the collisional data, the disparities were even less. This was particularly pleasing as the CIV3
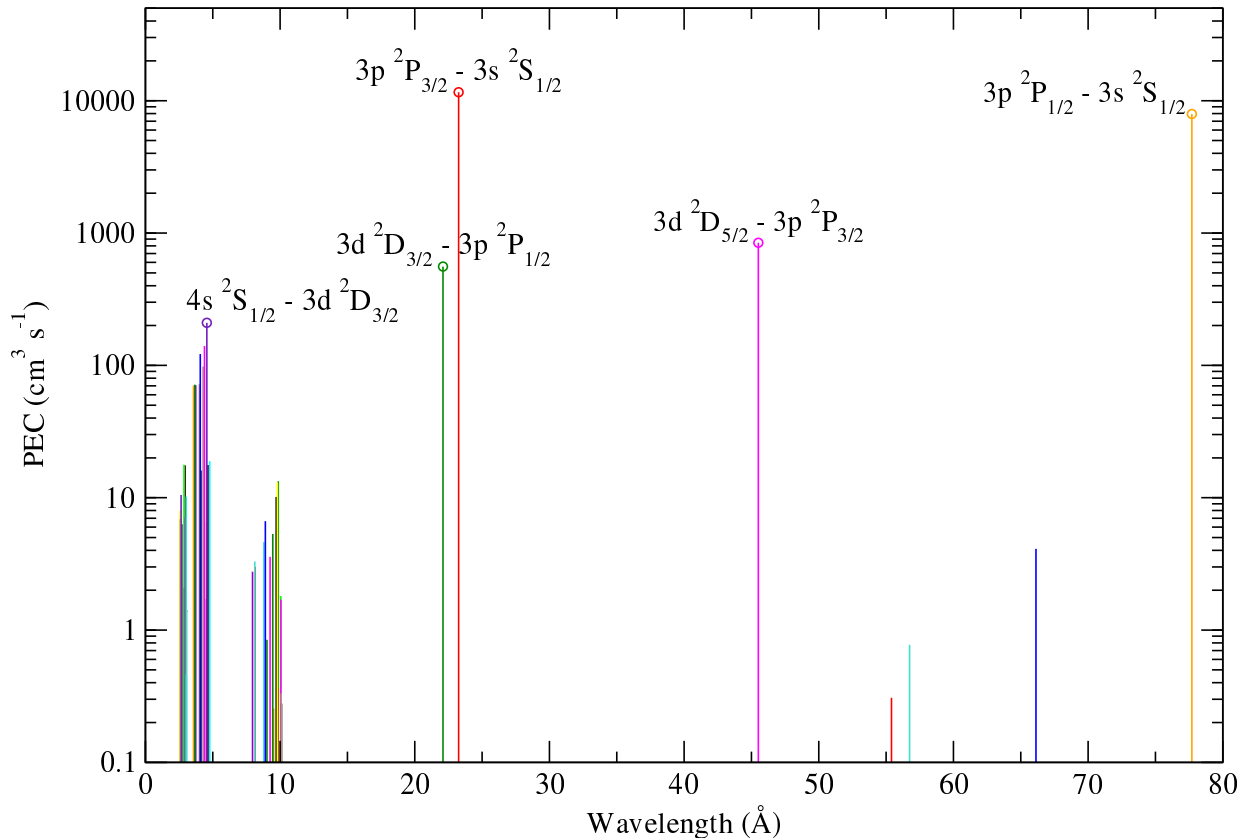
FIG. 6. A analysis of the photon emissivity coefficients (PECs) on the 0-80 Angstrom wavelength region for the W LXIV ion. The five strongest of these are annotated.

structure code orbital descriptions are not fully relativistic. We would not have expected CIV3 to give results which are, in many cases, so close to those from a fully relativistic code for such a highly ionised heavy system as W LXIV. However, as we have shown, for this system carefully defined and optimised CIV3 orbital parameters can be adopted to give accurate wavefunction descriptions. We [24] found for zinc-like W XLV, with two valence electrons, a simiarly modified set of radial functions from CIV3 was able to give a good representation of the fully relativistic description of the ion. We would like to investigate a more complicated tungsten system in the future, one which involves several electrons outside a closed core, to verify these findings further.

[1] Pitts R A, Carpentier S, Escourbiac F, Hirai T, Komarov V *et al.*2013, *J. Nucl. Mater.* **438** S48-S56

[2] Ballance C P, Loch S D, Pindzola M S and Griffin D C 2013, *J. Phys. B: At. Mol. Opt. Phys.* **46** 055202

[3] Safranova U I, Safranova A S and Beiersdorfer P 2009, *At. Data Nucl. Tables* **95** (5) 751-785

[4] Aggarwal K M and Keenan F P 2014, *At. Data Nucl. Tables* **100** (6) 1399-1518

[5] Kramida A E and Shirai T 2009, *At. Data Nucl. Data Tables* **95** 305-474

[6] Dipti, Tapasi D, Sharma L and S Rajesh 2014, *Phys. Scr.* **89** 085403

[7] Hibbert A 1975, *Comput. Phys. Commun.* **9** 141-172

[8] Hibbert A, Glass R, Froese Fischer C 1991, *Comput. Phys. Commun.* **64** 455-472

[9] Grant I P, McKenzie B J, Norrington P H, Mayers D F, and Pypner N C 1980, *Comput. Phys. Commun.* **21(2)** 207-231

[10] McKenzie B J, Grant I P, and Norrington P H 1980, *Comput. Phys. Commun.* **21(2)** 233-246

[11] Dyall K G, Grant I, Johnson C T, Parpia F A, and Plummer E P 1989, *Comput. Phys. Commun.* **55(3)** 425-256

[12] Griffin D C, Badnell N R and Pindzola M S 1998, *J. Phys. B: At. Mol. Opt. Phys.* **31** 3713-3727

[13] Burke P G, Burke V M and Dunseath K M 1994, *J. Phys. B: Mol. Opt. Phys.* **27** 5341-5373

[14] Perkins J F 1965, *J. Chem. Phys.* **45** 2156

[15] McLean A D and McLean R S 1981, *At. Data Nucl. Data Tables* **26** 197-381

[16] Burgess A and Tully J A 1992, *Astron. Astrophys.* **254** 436

[17] Whiteford A D, Badnell N R, Ballance C P, O'Mullane M G, Summers H P and Thomas A L 2001, *J. Phys. B: At. Mol. Opt. Phys.* **34** 3179

[18] Ballance C P and Griffin D C 2004, *J. Phys. B: At. Mol. Opt. Phys.* **37** 2943

[19] Mitnik D M, Griffin D C, Ballance C P and Badnell N R 2003, *J. Phys. B: At. Mol. Opt. Phys.* **36** 717

[20] Norrington P H 2004, www.am.qub.ac.uk/DARC

[21] Burgess A, Hummer D G and Tully J A 1970, *Phil. Trans. R. Soc. A* **266** 225-79

[22] Robicheaux F, Gorczyca T W, Pindzolda M S and Badnell N R 1995, *Phys. Rev. A.* **52** 1319

[23] Summers H P, Badnell N R, O'Mullane M G, Whiteford A D, Bingham R, Kellett B J, Lang J, Behringer K H, Fantz U, Zastrow K-D, Loch S D, Pindzola M S, Griffin D C and Ballance C P 2002, *Plasma Phys. Control. Fusion* **44** B323-B338

[24] Spencer S, Hibbert S and Ramsbottom C A 2014, *J. Phys. B: At. Mol. Opt.* **47** 245001